Microscopic Investigation into the Electric Field Effect on Proximity-Induced Magnetism in Pt

K. T. Yamada,[1] M. Suzuki,[2] A.-M. Pradipto,[1,3] T. Koyama,[4] S. Kim,[1] K.-J. Kim,[1] S. Ono,[5] T. Taniguchi,[1] H. Mizuno,[1] F. Ando,[1] K. Oda,[1] H. Kakizakai,[1] T. Moriyama,[1] K. Nakamura,[3] D. Chiba,[4,*] and T. Ono[1,6,†]

[1]*Institute for Chemical Research, Kyoto University, Uji, Kyoto 611-0011, Japan*
[2]*Japan Synchrotron Radiation Research Institute, Sayo, Hyogo 679-5198, Japan*
[3]*Department of Physics Engineering, Mie University, Tsu, Mie 514-8507, Japan*
[4]*Department of Applied Physics, The University of Tokyo, Bunkyo, Tokyo 113-8656, Japan*
[5]*Central Research Institute of Electric Power Industry, Yokosuka, Kanagawa 240-0196, Japan*
[6]*Center for Spintronics Research Network (CSRN), Graduate School of Engineering Science, Osaka University, Toyonaka, Osaka 560-8531, Japan*

(Received 13 June 2017; published 12 April 2018)

Electric field effects on magnetism in metals have attracted widespread attention, but the microscopic mechanism is still controversial. We experimentally show the relevancy between the electric field effect on magnetism and on the electronic structure in Pt in a ferromagnetic state using element-specific measurements: x-ray magnetic circular dichroism (XMCD) and x-ray absorption spectroscopy (XAS). Electric fields are applied to the surface of ultrathin metallic Pt, in which a magnetic moment is induced by the ferromagnetic proximity effect resulting from a Co underlayer. XMCD and XAS measurements performed under the application of electric fields reveal that both the spin and orbital magnetic moments of Pt atoms are electrically modulated, which can be explained not only by the electric-field-induced shift of the Fermi level but also by the change in the orbital hybridizations.

DOI: 10.1103/PhysRevLett.120.157203

Electrostatic carrier doping is a fundamental technology to manipulate electronic and magnetic properties in condensed matter [1]. The modulation of the carrier density and optimized Fermi level E_F by an electric field, for instance, induces distinguished electronic properties in strongly correlated oxides [2,3] and topological insulators [4,5]. The magnetic properties that are characterized by the carrier density and E_F position can also be controlled by an electric field in ferromagnetic semiconductors [6–9] and metals [9–14]. The electric field changes representative magnetic properties such as magnetic anisotropy [11] and Curie temperature [12], the latter of which is expected to realize an efficient magnetization reversal [13,14], writing operation, in magnetic recording media. Despite the interesting physics and potential applications, the microscopic mechanism has been experimentally unaddressed in the case of ferromagnetic metals. This contrasts with the situation that, in semiconductors, both experimental [8] and theoretical [15] works have already proved that electrically modulated E_F dominates the change in the magnetism. However, in metals, because the electric field is shielded at a surface atomic layer attributed to the screening effect, the effect on magnetism cannot be explained simply by the variation of E_F as pointed out by theoretical calculations [16–18].

In this Letter, we experimentally demonstrate the relation between the electric field effect on magnetism and on the electronic structure in Pt in a ferromagnetic state using x-ray magnetic circular dichroism (XMCD) [19–25] and x-ray absorption spectroscopy (XAS) [26–28]. Stoner-enhanced paramagnetic metals, e.g., Pt and Pd, stacked with ferromagnetic metals have an induced magnetic moment because of the ferromagnetic proximity effect [22,23,25,29–31]. Recent studies have demonstrated that an electric field can modulate the proximity-induced magnetism in Pd [30,31]. XMCD and XAS are powerful techniques to detect magnetism and the electronic structure of a specific element. An XMCD spectrum includes information regarding the magnetic polarization and the difference in empty density of states (DOSs) between the minority and majority bands. Furthermore, applying sum rules [32,33] to XMCD spectra makes it possible to evaluate the spin and orbital magnetic moments separately. Moreover, we can examine the electronic structure using the XAS integral that is proportional to the unoccupied states. The XMCD spectra measured under the application of electric fields clearly demonstrate that the spin and the orbital magnetic moments in the Pt atom are electrically modulated. The agreement of the experimental XMCD and XAS spectra with those obtained using density function theory (DFT) calculations suggests that the shift of E_F and the change in the orbital hybridizations by the electric field application result in the modulation of magnetism in the present metallic system.

In order to investigate the electric field effect on magnetism using XMCD and XAS, we fabricated an electric double-layer [34–38] capacitor with a metallic Pt ultrathin film in a ferromagnetic state. The schematic illustration of the electric double-layer capacitor is summarized in Fig. 1(a). Pd(4.0 nm)/Co(0.5 nm)/Pt(0.4 nm) with a 2.0-nm-thick MgO cap layer was deposited onto a glass substrate by rf sputtering. This multilayer shows a perpendicular easy axis of magnetization. The orbital hybridizations between the Pt and ferromagnetic Co underlayer atoms result in the magnetic polarization of Pt. The multilayer was first processed into a 1.0 mm × 0.5 mm channel, which corresponds to the Pt electrode for the electric double-layer capacitor, fabricated by photolithography and Ar-ion milling. Next, two gate electrodes and electrodes for electrical contacts made of Ti(5 nm)/Au(100 nm) were formed in the lateral side of the Pt electrode by a lift-off process. The total area of the two gate electrodes was 5 mm^2. Then, a 50-nm-thick SiO_2 layer was deposited on a region excluding the channel and electrodes. Finally, both the gate electrodes and the Pt electrode in between were covered by an ionic liquid (IL) of N, N-diethyl-N-(2-methoxyethyl)-N-methylammonium bis (trifluoromethylsulphonyl) imide (DEME-TFSI). The application of the gate voltage V_G attracts ions on the MgO surface and results in an accumulation of charges at the Pt surface; i.e., an electric double layer is formed. Here, a positive (negative) V_G results in an increase (decrease) in the electron density at the Pt surface. The electric field strength corresponding to $|V_G| = 1$ V is estimated to be ~0.3 V/nm by assuming the effective dielectric thickness of the IL of ~1 nm [35] and the MgO thickness of 2 nm; thus, the total dielectric thickness of the present electric double-layer capacitor (IL + MgO) is ~3 nm [36]. See Supplemental Material for details of the material and device [39].

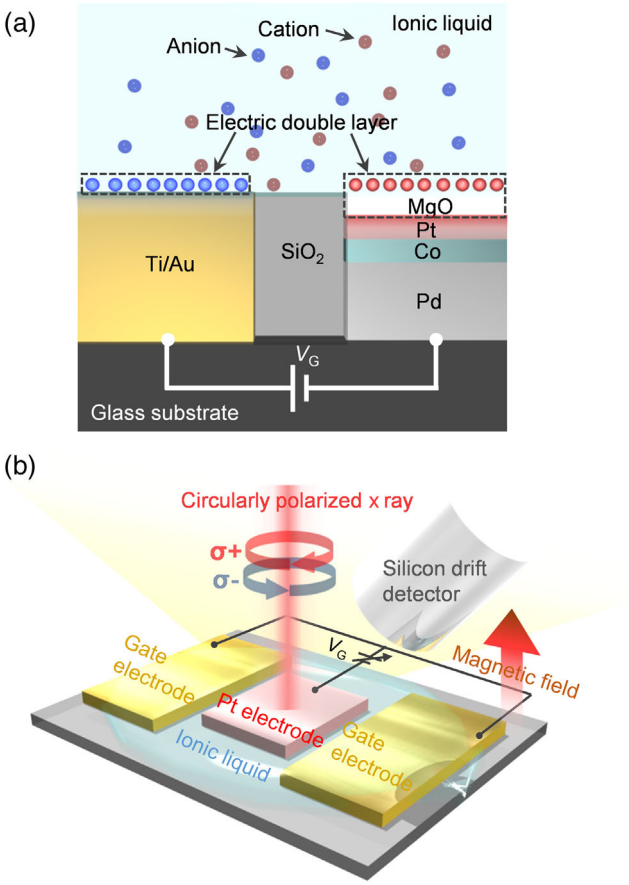

FIG. 1. (a) Schematic cross section of the electric double-layer capacitor. The ionic liquid is used to apply the electric field to the surface of the ferromagnetic Pt layer. (b) Schematic image of the measurement configuration for XMCD and XAS.

XMCD and XAS measurements were performed at BL39XU of the SPring-8 synchrotron radiation facility, where a circularly polarized hard x-ray beam to investigate magnetically polarized Pt is available. Here, we used the photon-in–photon-out technique, florescence yield mode, allowing stable data acquisition even under an electric field application with a high signal-to-noise ratio. The photon-in–electron-out technique, electron yield mode, is not suitable for hard XMCD and XAS measurements because of the very small photoelectron yield for a transition from deep core levels. A He-flowing cryostat was used to control the device temperature. The cryostat chamber was evacuated to ~10^{-4} Pa immediately after introducing the device. The device temperature had been maintained at 330 K before all XMCD and XAS measurements for 2 hr to remove chemical agents from the IL such as water and air, which are possible reactants for an undesired redox. The V_G was applied at 220 K, which was a little above the glass transition temperature of the IL (DEME-TFSI) [37,38]. Then, the device was cooled down to 100 K to prevent the IL from being damaged by x-ray irradiation. Subsequently, the energy scan was conducted three times at different positions on the channel to minimize damage to the film and IL from the incident x ray, and three spectra curves were averaged.

Figure 1(c) displays a schematic image of the XMCD and XAS measurement configuration.

A circularly polarized x-ray beam with a high degree of circular polarization (≥95%) being incident on the Pt electrode produces the x-ray florescence from the Pt atoms depending on the x-ray photon helicity and the magnetization direction. The incidence and florescence x ray can penetrate the IL owing to the high energy; namely, the targeted atoms under the IL are measurable not by soft x ray but by hard x ray. During the XMCD and XAS measurements, the magnetic field was applied along the normal direction to the film plane. The x-ray photon helicities were switched at every energy point at 0.5 Hz. The x-ray fluorescence yields resulting from the x-ray absorption of Pt were observed using a four-element silicon drift detector (Sirius 4, SGX Sensortech Inc.), with an effective area of 65 mm^2 for each detector element. The output pulse signals from the detector were processed using an X-map

(XIA Inc.). Intensities of the Pt L_α and Pt L_β lines were monitored as a function of the x-ray energy at the Pt L_3 and L_2 edges, respectively. The outputs from four detector channels were accumulated for 10.0 s for each helicity, and the total photon counts were ~270 000 count at each energy point. The XAS and XMCD intensities are defined as $I_{\mathrm{XAS}} = [I(\sigma^+) + I(\sigma^-)]/2$ and $I_{\mathrm{XMCD}} = I(\sigma^+) - I(\sigma^-)$, respectively, where $I(\sigma^+)$ and $I(\sigma^-)$ indicate the intensities of x-ray fluorescence when the incident photon momentum and the magnetization vectors are antiparallel and parallel, respectively. The obtained XMCD and XAS spectra were normalized by the edge step height of the XAS spectra and multiplied by 2.22 at the L_3 edge and 1.0 at the L_2 edge [22–24].

The XMCD spectra for $V_G = +6$ and -4 V and their difference (ΔI_{XMCD}) measured under the perpendicular magnetic field of 0.6 T at 100 K are shown in Fig. 2(a). These V_G's corresponded to electric fields of $+1.8$ and -1.2 V/nm at the Pt surface, respectively. The I_{XMCD} at the L_3 edge ($2p_{3/2}$ core → $5d$ valence) shows a small but finite difference between different V_G's as can be seen in the magnified view [see the inset in Fig. 2(a)]. In contrast, a finite difference is not observed at the L_2 edge ($2p_{1/2}$ core → $5d$ valence), which can be seen as well in ΔI_{XMCD} around the edge; i.e., the change is below the noise level. This asymmetric modulation at the L_3 and L_2 edges provides evidence that the orbital magnetic moment $m_o^\perp$ for the perpendicular magnetization direction is modulated by the V_G application. Figure 2(b) shows the XAS for $V_G = +6$ and -4 V and their difference (ΔI_{XAS}). The clear difference is found also in ΔI_{XAS}, suggesting that the number of $5d$ holes n_h is changed by V_G. The sum of integration values of ΔI_{XAS} around the L_3 and L_2 edges is ~ -0.18 eV, equivalent to the decrease in n_h ($\Delta n_h \sim -0.009$), indicating that the positive V_G increases the electron occupation of the $5d$ states. Notably, Fig. 2(b) indicates that there is a change in the sign of ΔI_{XAS} at the L_3 and L_2 absorption edges: The ΔI_{XAS} is negative at low-energy sides of the white line peaks of I_{XAS} at the L_3 (11.571 keV) and L_2 (13.283 keV) edges and becomes positive at the high-energy sides. This means that the number of the unoccupied states decreases in the vicinity of the E_F by the application of the positive V_G, most likely pushing up the E_F. On the other hand, the ΔI_{XAS} also changes sign around 11.571 eV, about 20 eV above the threshold of the L_3 edge. ΔI_{XAS} shows a positive peak at 11.572 keV and a negative peak at 11.568 keV, for which the application of V_G probably changes the orbital hybridization between unoccupied $5d$ and $6s$ and/or $6p$ orbitals as discussed below. At the L_2 edge, there are corresponding sign changes of the ΔI_{XAS} around 13.290 keV. Therefore, the obtained results suggest that the electric field effect on magnetism observed here results from two different mechanisms, i.e., the shift of E_F and the change in the orbital hybridization. Very recently, Miwa *et al.* [47] have reported voltage-induced changes in the XMCD and XAS spectra of Pt in a $L1_0$-FePt/MgO junction. They revealed that an electric field induction of an electric quadrupole, which produces a magnetic dipole moment [40–42] in the Pt $5d$ orbit, can be a dominant source of the voltage-induced magnetic anisotropy in the system; in contrast, we have performed the thorough spectroscopy study to unravel the microscopic mechanism of the electric field effect on magnetism in the Pt in a ferromagnetic state.

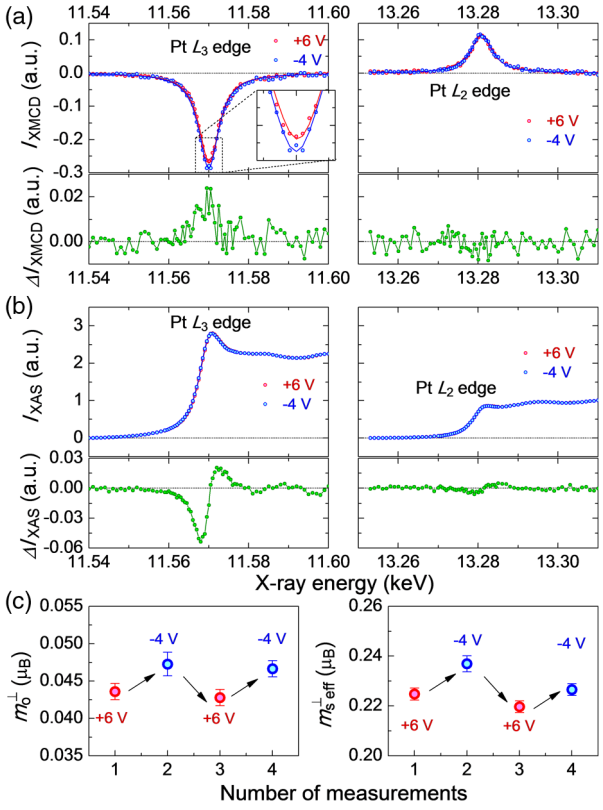

FIG. 2. (a) The XMCD intensities I_{XMCD} at Pt L_3 and L_2 edges for $V_G = +6$ and -4 V (upper panels) and their difference $\Delta I_{\mathrm{XMCD}}[=I_{\mathrm{XMCD}}(+6\ \mathrm{V}) - I_{\mathrm{XMCD}}(-4\ \mathrm{V})]$ (bottom panels). (b) The XAS intensities I_{XAS} at Pt L_3 and L_2 edges for $V_G = +6$ and -4 V (upper panels) and their difference $\Delta I_{\mathrm{XAS}}[=I_{\mathrm{XAS}}(+6\ \mathrm{V}) - I_{\mathrm{XMCD}}(-4\ \mathrm{V})]$ (bottom panels). (c) The orbital and the effective spin magnetic moments ($m_o^\perp$ and $m_{s,\mathrm{eff}}^\perp$, shown in the right and left panels, respectively) determined using the sum rules [32,33]. The horizontal axis corresponds to the number of measurements, where V_G is changed in the order of $+6 \rightarrow -4 \rightarrow +6 \rightarrow -4$ V.

The electric field effect on the electronic structure is directly observed, and a qualitative understanding is obtained. We then quantitatively determine the values of orbital $m_o^\perp$ and effective spin magnetic moment $m_{s,\mathrm{eff}}^\perp$ for the perpendicular magnetization direction by using the sum rules. See Supplemental Material for details of the sum-rule analysis [39]. We determined $m_o^\perp = 0.043 \pm 0.001 (0.047 \pm 0.001)\mu_B$ and $m_{s,\mathrm{eff}}^\perp = 0.222 \pm 0.001 (0.232 \pm 0.002)\mu_B$ for $V_G = +6(-4)$ V, respectively, with a

precision of $0.002\mu_B$. The absolute values of the magnetic moments obtained from our analysis should have an accuracy of 5%–10%, which is mainly due to systematic errors in the hole number, in the degree of circular polarization, and in the estimation of the white line integrals. On the other hand, the precision of the magnetic moment values determined from the spectra measured in identical conditions was better than 1%, because we obtained very smooth XMCD and XAS spectra with extremely high reproducibility. Thus, we can discuss relative changes of the order of 1% in the magnetic moment values for different V_G's.

To check the reproducibility of the result under the gating, the measurements were repeated in the same way for V_G in the order of $+6 \rightarrow -4 \rightarrow +6 \rightarrow -4$ V. The values obtained in the repeated measurements are plotted in Fig. 2(c), which confirms that the change is reversible and reproducible. From the detailed analysis, we checked that voltage-induced redox reactions [43,44] are not dominant for the present device (see Supplemental Material [39]). This is probably because the ionization tendency of Pt is low and the application of V_G was performed at a temperature low enough to suppress the pseudocapacitance of the IL derived from the redox reactions [38].

Finally, we discuss the mechanism for the electric field effect observed here using the theoretical calculations based on the DFT (for detail, see Supplemental Material [39] and Refs. [45,46]). Figures 3(b) and 3(b) show the calculated I_{XMCD} and I_{XAS} spectra in the case for the perpendicularly magnetized Pt. The I_{XMCD} and I_{XAS} spectra were calculated within the approximation of electric dipole transitions under electric fields of ± 10 V/nm, respectively, by employing a slab model depicted in the inset in Fig. 3(a). The differences of the spectra are shown together. The characteristic features of the calculated spectra and those differences show good agreement with the experimental results shown in Figs. 2(a) and 2(b). The asymmetric change in the $|\Delta I_{\mathrm{XMCD}}|$ around the L_3 and L_2 edges indicates that the orbital polarization around E_F is modulated. The calculated orbital ($m_o^{\perp}$) and spin (m_s) magnetic moment for the applied fields of $+10(-10)$ V/nm are $0.034\,(0.035)\mu_B$ and $0.195\,(0.198)\mu_B$, respectively. The calculated magnitudes of the changes are slightly smaller than the experimental values, but the direction of the changes agrees with the experiments. Although the sputter-deposited thin Pt is probably islandlike, a qualitative agreement between the experiment and DFT calculation is found. One plausible explanation for this qualitative agreement is that the stack of the Pt island, which is anticipated to be (111) oriented since Pt is a fcc metal, is close to the model used in the calculation, and only the Pt islands are measured by the element-specific x-ray techniques.

Figures 3(c) shows the differences of the DOSs calculated for the positive and negative electric fields for $6s$, $6p$, and $5d$ orbitals. Two important points can be discerned:

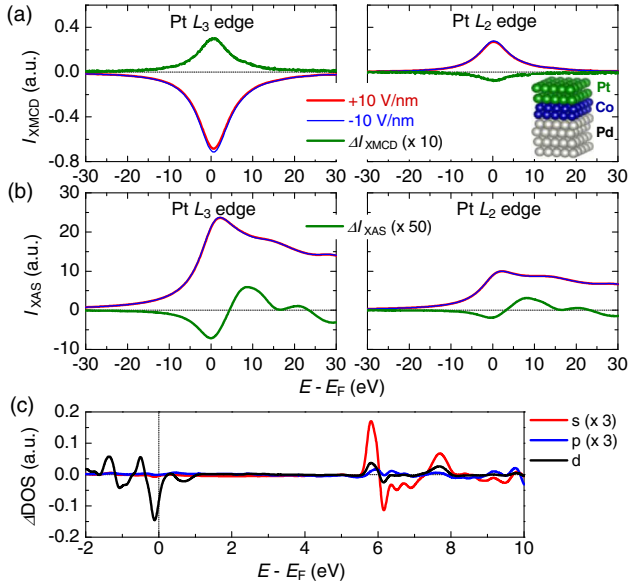

FIG. 3. (a) The calculated I_{XMCD} spectra around Pt L_3 and L_2 edges for the electric field of ± 10 V/nm and their difference $\Delta I_{\mathrm{XMCD}}[=I_{\mathrm{XMCD}}(+10\ \mathrm{V/nm}) - I_{\mathrm{XMCD}}(-10\ \mathrm{V/nm})]$. ΔI_{XMCD} is magnified by a factor of 10. The inset shows the slab model used that consisted of a Pd (four MLs)/Co (two MLs)/Pt (two MLs) from the bottom side (ML, monolayer). The electric field is applied to the surface of the Pt layer. (b) The calculated I_{XAS} spectra around Pt L_3 and L_2 edges for the electric field of ± 10 V/nm and their difference $\Delta I_{\mathrm{XAS}}[=I_{\mathrm{XAS}}(+10\ \mathrm{V/nm}) - I_{\mathrm{XAS}}(-10\ \mathrm{V/nm})]$. ΔI_{XAS} is magnified by a factor of 50. (c) The differences of the densities of states (ΔDOS) calculated for the positive and negative electric fields (± 10 V/nm). The lines indicate the ΔDOS for $6s$, $6p$, and $5d$ orbitals, and those for s and p orbitals are magnified by a factor of 3.

First, the application of the positive electric field decreases the $5d$ states around the E_F. The eigenstates of all the $5d$ and $6sp$ orbitals shift down in parallel towards lower (higher) energy with respect to the E_F by the positive (negative) electric field, as displayed in Fig. S3 [39], which arises from the E_F shift through the electron accumulation (depletion). Second, in contrast, the application of the positive electric field increases the $5d$, $6s$, and $6p$ states at ~6 eV above E_F. The energy shift of the antibonding states at around 6 eV above the E_F, mainly consisting of the $6sp$ orbitals, is larger than that of the bonding states (Fig. S3, [39]). This indicates that the antibonding $6sp$ states are pushed down (up) in energy with respect to the bonding $5d$ state by the positive (negative) electric field. Thus, the modification of the $5d$-$6sp$ hybridizations is additionally modified by the introduction of an electric field [16,18].

To see moreover the two distinct mechanisms, i.e., the electric-field-induced shift in E_F and change in orbital hybridization, in Supplemental Material Sec. VI [39], we quantified the relative contributions to the hole number and magnetic moment, where the modification of the electronic structure only by the E_F shift was mimicked by artificially

shifting the E_F of the electronic structure at a zero electric field. When the electric field is switched from -10 to $+10$ V/nm, the modulated orbital hybridization increases the n_h; in contrast, the elevated E_F decreases the n_h. Both the mechanisms increase the m_s. Those variations by the latter mechanism can be comparable to those by the former mechanism. Although a recent theoretical calculation [48] suggests that an electric field modulation of the magnetic anisotropy in $3d$ ferromagnetic metals is qualitatively explained by electron injection and depletion, i.e., E_F shift, the present quantitative study corroborates the importance of the electrical modification of orbital hybridization.

The highly sensitive XMCD and XAS experiments have showed that an electric field applied to a magnetically polarized Pt layer can modulate both the orbital and spin magnetic moment; for more significance, the microscopic mechanisms, i.e., the shift of the position of E_F and the change in the orbital hybridization, have been experimentally unraveled for the first time. The microscopic mechanism of the electric field effect on magnetism elucidated here using a ferromagnetic Pt would provide us with a fundamental model that is applicable to a wide range of ferromagnetic metals, e.g., the electric-field-induced change in the magnetic anisotropy [13] and the change in the Curie temperature [14] in $3d$ transition metal/MgO structures, where a similar mechanism has been proposed based on theoretical calculations [16,18].

We thank M. Kawaguchi and K. Miwa for fruitful discussions. K. T. Y. was supported by the Japan Society for the Promotion of Science (JSPS) through a research fellowship for young scientists (Grant No. 14J08822). This work was partly supported by Grants-in-Aid for Specially Promoted Research, Scientific Research (S), and Scientific Research on Innovative Area, "Nano Spin Conversion Science" (Grants No. 15H05702, No. 25220604, and No. 26103002, respectively) from JSPS, ImPACT Program of CSTI, Spintronics Research Network of Japan, and Collaborative Research Program of the Institute for Chemical Research, Kyoto University. The synchrotron radiation experiments were performed at SPring-8 with the approval of the Japan Synchrotron Radiation Research Institute (JASRI) (Proposals No. 2015A0125, No. 2015B0125, No. 2016A0125, No. 2016B0125, No. 2015B0901, No. 2016A0901, and No. 2016B0901/BL39XU).

*Corresponding author.
dchiba@ap.t.u-tokyo.ac.jp
†ono@scl.kyoto-u.ac.jp

[1] C. H. Ahn, A. Bhattacharya, M. D. Ventra, J. N. Eckstein, C. D. Frisbie, M. E. Gershenson, A. M. Goldman, I. H. Inoue, J. Mannhart, A. J. Millis, A. F. Morpurgo, D. Natelson, and J. M. Triscone, Rev. Mod. Phys. **78**, 1185 (2006).
[2] M. Imada, A. Fujimori, and Y. Tokura, Rev. Mod. Phys. **70**, 1039 (1998).
[3] K. Ueno, K. Ueno, S. Nakamura, H. Shimotani, A. Ohtomo, N. Kimura, T. Nojima, H. Aoki, Y. Iwasa, and M. Kawasaki, Nat. Mater. **7**, 855 (2008).
[4] X.-L. Qi and S.-C. Zhang, Rev. Mod. Phys. **83**, 1057 (2011).
[5] D. Kong, Y. Chen, J. J. Cha, Q. Zhang, J. G. Analytis, K. Lai, Z. Liu, S. S. Hong, K. J. Koski, S.-K. Mo, Z. Hussain, I. R. Fisher, Z.-X. Shen, and Y. Cui, Nat. Nanotechnol. **6**, 705 (2011).
[6] H. Ohno, D. Chiba, F. Matsukura, T. Omiya, E. Abe, T. Dietl, Y. Ohno, and K. Ohtani, Nature (London) **408**, 944 (2000).
[7] D. Chiba, M. Sawicki, Y. Nishitani, Y. Nakatani, F. Matsukura, and H. Ohno, Nature (London) **455**, 515 (2008).
[8] M. Sawicki, D. Chiba, A. Korbecka, Y. Nishitani, J. A. Majewski, F. Matsukura, T. Dietl, and H. Ohno, Nat. Phys. **6**, 22 (2010).
[9] F. Matsukura, Y. Tokura, and H. Ohno, Nat. Nanotechnol. **10**, 209 (2015).
[10] M. Weisheit, S. Fähler, A. Marty, Y. Souche, C. Poinsignon, and D. Givord, Science **315**, 349 (2007).
[11] T. Maruyama, Y. Shiota, T. Nozaki, K. Ohta, N. Toda, M. Mizuguchi, A. A. Tulapurkar, T. Shinjo, M. Shiraishi, S. Mizukami, Y. Ando, and Y. Suzuki, Nat. Nanotechnol. **4**, 158 (2009).
[12] D. Chiba, S. Fukami, K. Shimamura, N. Ishiwata, K. Kobayashi, and T. Ono, Nat. Mater. **10**, 853 (2011).
[13] Y. Shiota, T. Nozaki, F. Bonell, S. Murakami, T. Shinjo, and Y. Suzuki, Nat. Mater. **11**, 39 (2012).
[14] S. Kanai, M. Yamanouchi, S. Ikeda, Y. Nakatani, F. Matsukura, and H. Ohno, Appl. Phys. Lett. **101**, 122403 (2012).
[15] T. Dietl, H. Ohno, F. Matsukura, J. Cibert, and D. Ferrand, Science **287**, 1019 (2000).
[16] K. Nakamura, R. Shimabukuro, Y. Fujiwara, T. Akiyama, T. Ito, and A. J. Freeman, Phys. Rev. Lett. **102**, 187201 (2009).
[17] M. Tsujikawa and T. Oda, Phys. Rev. Lett. **102**, 247203 (2009).
[18] M. Oba, K. Nakamura, T. Akiyama, T. Ito, M. Weinert, and A. J. Freeman, Phys. Rev. Lett. **114**, 107202 (2015).
[19] G. Schütz, W. Wagner, W. Wilhelm, P. Kienle, R. Zeller, R. Frahm, and G. Materlik, Phys. Rev. Lett. **58**, 737 (1987).
[20] J. Stöhr, J. Electron Spectrosc. Relat. Phenom. **75**, 253 (1995).
[21] R. Wu, D. Wang, and A. J. Freeman, J. Magn. Magn. Mater. **132**, 103 (1994).
[22] W. Grange, M. Maret, J.-P. Kappler, J. Vogel, A. Fontaine, F. Petroff, G. Krill, A. Rogalev, J. Goulon, M. Finazzi, and N. B. Brookes, Phys. Rev. B **58**, 6298 (1998).
[23] M. Suzuki, H. Muraoka, Y. Inaba, H. Miyagawa, N. Kawamura, T. Shimatsu, H. Maruyama, N. Ishimatsu, Y. Isohama, and Y. Sonobe, Phys. Rev. B **72**, 054430 (2005).
[24] J. Bartolomé, F. Bartolomé, L. M. García, E. Roduner, Y. Akdogan, F. Wilhelm, and A. Rogalev, Phys. Rev. B **80**, 014404 (2009).
[25] C. Ederer, M. Komelj, M. Fähnle, and G. Schütz, Phys. Rev. B **66**, 094413 (2002).

[26] E. Tamura, J. van Ek, M. Fröba, and J. Wong, Phys. Rev. Lett. **74**, 4899 (1995).
[27] S. Mukerjee, S. Srinivasan, M. P. Soriaga, and J. McBreen, J. Electrochem. Soc. **142**, 1409 (1995).
[28] S. Miwa, K. Matsuda, K. Tanaka, Y. Kotani, M. Goto, T. Nakamura, and Y. Suzuki, Appl. Phys. Lett. **107**, 162402 (2015).
[29] R. Wu, C. Li, and A. J. Freeman, J. Magn. Magn. Mater. **99**, 71 (1991).
[30] Y. Hibino, T. Koyama, A. Obinata, K. Miwa, S. Ono, and D. Chiba, Appl. Phys. Express **8**, 113002 (2015).
[31] A. Obinata, Y. Hibino, D. Hayakawa, T. Koyama, K. Miwa, S. Ono, and D. Chiba, Sci. Rep. **5**, 14303 (2015).
[32] B. T. Thole, P. Carra, F. Sette, and G. van der Laan, Phys. Rev. Lett. **68**, 1943 (1992).
[33] P. Carra, B. T. Thole, M. Altarelli, and X. Wang, Phys. Rev. Lett. **70**, 694 (1993).
[34] M. A. V. Devanathan and B. V. K. S. R. A. Tilak, Chem. Rev. **65**, 635 (1965).
[35] R. Yamamoto, H. Morisaki, O. Sakata, H. Shimotani, H. Yuan, Y. Iwasa, T. Kimura, and Y. Wakabayashi, Appl. Phys. Lett. **101**, 053122 (2012).
[36] D. Hayakawa, A. Obinata, K. Miwa, S. Ono, T. Hirai, T. Koyama, and D. Chiba, AIP Adv. **6**, 115305 (2016).
[37] T. Sato, G. Masuda, and K. Takagi, Electrochim. Acta **49**, 3603 (2004).
[38] H. Yuan, H. Shimotani, J. Ye, S. Yoon, H. Aliah, A. Tsukazaki, M. Kawasaki, and Y. Iwasa, J. Am. Chem. Soc. **132**, 18402 (2010).
[39] See Supplemental Material at http://link.aps.org/supplemental/10.1103/PhysRevLett.120.157203 for details about the material and device, sum-rule analysis and DFT calculation, evaluation of the possibility of redox reactions, calculated electronic structures, and evaluating relative contributions of the E_F shift and change in orbital hybridization to the hole number and magnetic moment, which includes Refs. [22,24,32,33,40–46].
[40] J. Stöhr and H. König, Phys. Rev. Lett. **75**, 3748 (1995).
[41] G. van der Laan, J. Phys. Condens. Matter **10**, 3239 (1998).
[42] T. Oguchi and T. Shishidou, Phys. Rev. B **70**, 024412 (2004).
[43] C. Bi, Y. Liu, T. Newhouse- Illige, M. Xu, M. Rosales, J. W. Freeland, O. Mryasov, S. Zhang, S. G. E. te Velthuis, and W. G. Wang, Phys. Rev. Lett. **113**, 267202 (2014).
[44] U. Bauer, L. Yao, A. J. Tan, P. Agrawal, S. Emori, H. L. Tuller, S. van Dijken, and G. S. D. Beach, Nat. Mater. **14**, 174 (2015).
[45] K. Nakamura, T. Ito, A. J. Freeman, L. Zhong, and J. Fernandez-de-Castro, Phys. Rev. B **67**, 014420 (2003).
[46] M. Weinert, G. Schneider, R. Podloucky, and J. Redinger, J. Phys. Condens. Matter **21**, 084201 (2009).
[47] S. Miwa, M. Suzuki, M. Tsujikawa, K. Matsuda, T. Nozaki, K. Tanaka, T. Tsukahara, K. Nawaoka, M. Goto, Y. Kotani, T. Ohkubo, F. Bonell, E. Tamura, K. Hono, T. Nakamura, M. Shirai, S. Yuasa, and Y. Suzuki, Nat. Commun. **8**, 15848 (2017).
[48] J. Zhang, P. V. Lukashev, S. S. Jaswal, and E. Y. Tsymbal, Phys. Rev. B **96**, 014435 (2017).